

1 **A large role of missing volatile organic compounds reactivity**  
2 **from anthropogenic emissions in ozone pollution regulation**

3 Wenjie Wang<sup>1,2\*</sup>, Bin Yuan<sup>1\*</sup>, Hang Su<sup>2</sup>, Yafang Cheng<sup>2</sup>, Jipeng Qi<sup>1</sup>, Sihang Wang<sup>1</sup>,  
4 Wei Song<sup>3</sup>, Xinming Wang<sup>3</sup>, Chaoyang Xue<sup>2</sup>, Chaoqun Ma<sup>2</sup>, Fengxia Bao<sup>2</sup>, Hongli  
5 Wang<sup>4</sup>, Shengrong Lou<sup>4</sup>, Min Shao<sup>1</sup>

6 <sup>1</sup> Institute for Environmental and Climate Research, Jinan University,  
7 Guangzhou 511443, China

8 <sup>2</sup> Multiphase Chemistry Department, Max Planck Institute for Chemistry, Mainz  
9 55128, Germany

10 <sup>3</sup> State Key Laboratory of Organic Geochemistry, Guangzhou Institute of  
11 Geochemistry, Chinese Academy of Sciences, Guangzhou 510640, China

12 <sup>4</sup> State Environmental Protection Key Laboratory of Formation and Prevention of  
13 Urban Air Pollution Complex, Shanghai Academy of Environmental Sciences,  
14 Shanghai 200233, China

15

16

17 *\*Correspondence to:* Bin Yuan ([byuan@jnu.edu.cn](mailto:byuan@jnu.edu.cn));  
18 Wenjie Wang ([Wenjie.Wang@mpic.de](mailto:Wenjie.Wang@mpic.de))

19

20 **Abstract:** There are thousands of VOC species in ambient air, while existing techniques  
21 can only detect a small part of them (~ several hundred). The large number of  
22 unmeasured VOCs prevents us from understanding the photochemistry of ozone and  
23 aerosols in the atmosphere. The major sources and photochemical effects of these  
24 unmeasured VOCs in urban areas remain unclear. The missing VOC reactivity, which  
25 is defined as the total OH reactivity of the unmeasured VOCs, is a good indicator to  
26 constrain the photochemical effect of unmeasured VOCs. Here, we identified the  
27 dominant role of anthropogenic emission sources in the missing VOC reactivity  
28 (accounting for up to 70%) by measuring missing VOC reactivity and tracer-based  
29 source analysis in a typical megacity in China. Omitting the missing VOC reactivity  
30 from anthropogenic emissions in model simulations will remarkably affect the  
31 diagnosis of sensitivity regimes for ozone formation, overestimating the degree of  
32 VOC-limited regime by up to 46%. Therefore, a thorough quantification of missing  
33 VOC reactivity from various anthropogenic emission sources is urgently needed for  
34 constraints of air quality models and the development of effective ozone control  
35 strategies.

36

37

## 38 **1 Introduction**

39 Volatile organic compounds (VOCs) are key precursors of major photochemical  
40 pollutants, including ozone ( $O_3$ ) and secondary organic aerosols (Atkinson,  
41 2000; Atkinson and Arey, 2003). Severe  $O_3$  and particle pollution are frequently related  
42 to high emissions of VOCs (Atkinson and Arey, 2003; Monks et al., 2015). There exist  
43 thousands of VOC species in ambient air that are emitted from either natural processes  
44 or anthropogenic activities (Goldstein and Galbally, 2007). No one instrument can  
45 capture all VOCs out there and even when they can be measured there is information  
46 missing on identification and properties (Yuan et al., 2017; Wang et al., 2014). Gas  
47 chromatograph–mass spectrometer/flame ionization detector (GC–MS/FID) can  
48 measure C<sub>2</sub>–C<sub>12</sub> non-methane hydrocarbons (NMHCs) and C<sub>2</sub>–C<sub>6</sub> oxygenated VOCs  
49 (OVOCs) while cannot measure NMHCs and OVOCs with larger carbon number  
50 (Wang et al., 2014). Proton-transfer-reaction time-of-flight mass spectrometer (PTR-  
51 ToF-MS) is able to measure a huge number of OVOCs and aromatics and several  
52 alkanes, but cannot measure most alkanes and alkenes, and cannot distinguish isomers  
53 (Yuan et al., 2017). The 2,4-dinitrophenylhydrazine (DNPH)/high performance liquid  
54 chromatography (HPLC) method can measure several carbonyls but cannot measure  
55 non-polar organic species (Wang et al., 2009). The two-dimensional GC is able to  
56 measure some intermediate-volatile and semi-volatile non-polar organics (Song et al.,  
57 2022). A lack of standard gases prevents these technologies from accurate  
58 quantification even if these technologies can identify more VOC species. In general,  
59 many branched alkenes, OVOCs with complex functional groups, intermediate-volatile  
60 and semi-volatile organics and complex biogenic VOCs cannot currently be well  
61 quantified even if they can be identified by instruments. As a result, the total amount of  
62 VOCs in ambient air has generally been underestimated. Currently, emission  
63 inventories used in air quality models such as the Community Emissions Data System  
64 (CEDS) emission inventory and the multi-resolution Emission Inventory for China  
65 (MEIC) only include the VOC species that can be measured such as some C<sub>1</sub>–C<sub>9</sub>

66 hydrocarbons and simple-structure OVOCs with small carbon number (<C6). This will  
67 lead to an underestimation of the photochemical effect of total VOCs and thus causes  
68 uncertainties in predicting secondary pollution. The quantification of the unmeasured  
69 VOCs is crucial to assess secondary pollution precisely.

70 The total OH reactivity ( $R_{OH}$ ), which can be directly measured, is an index for  
71 evaluating the amount of reductive pollutants in terms of ambient OH loss. The total  
72 OH reactivity is defined as:

$$73 \quad R_{OH} = \sum_i k_{OH+X_i} [X_i], \quad (1)$$

74 where  $X$  represents a reactive species including carbon monoxide (CO), nitrogen oxides  
75 (NO<sub>x</sub>) and VOCs etc., and  $k_{OH+X_i}$  is the reaction rate constant for the oxidation of  
76 species  $X$  by OH. The measured  $R_{OH}$  is higher than that calculated based solely on the  
77 measured reactive species, and the difference between them is mostly from unmeasured  
78 VOCs (Yang et al., 2017). Missing VOC reactivity (missing VOC<sub>R</sub>), defined as VOC  
79 reactivity (VOC<sub>R</sub>) of all unmeasured VOCs, can be obtained by subtracting the  
80 calculated  $R_{OH}$  from the measured  $R_{OH}$ .

$$81 \quad \text{missing VOC}_R = \text{measured } R_{OH} - \text{calculated } R_{OH} \quad (2)$$

$$82 \quad \text{calculated } R_{OH} = \sum_i k_{OH+reactive\ species_i} [reactive\ species_i] \quad (3)$$

83 where reactive species represents measured VOCs and reactive inorganic species  
84 including carbon monoxide (CO), nitric oxide (NO), nitrogen dioxide (NO<sub>2</sub>), O<sub>3</sub>, sulfur  
85 dioxide (SO<sub>2</sub>), nitrous acid (HONO), and so on. The missing VOC<sub>R</sub> provides a  
86 constraint for evaluating the photochemical roles of unmeasured VOCs in the  
87 atmosphere (Sadanaga et al., 2005; Yang et al., 2016b). The inclusion of the missing  
88 VOC<sub>R</sub> can help to improve the performance of box model and air quality models in  
89 simulating photochemistry processes. Relatively high missing VOC<sub>R</sub> have been found  
90 in forests (Di Carlo et al., 2004; Hansen et al., 2014; Nakashima et al., 2014; Nölscher et  
91 al., 2016; Praplan et al., 2019), urban areas (Shirley et al., 2006; Yoshino et al.,  
92 2006; Dolgorouky et al., 2012; Yang et al., 2017) and suburban areas (Kovacs et al.,  
93 2003; Yang et al., 2017; Fuchs et al., 2017; Lou et al., 2010), accounting for 10-75% of  
94 total  $R_{OH}$ . Given that total VOC<sub>R</sub> is one part of total  $R_{OH}$ , missing VOC<sub>R</sub> would account

95 for a larger percentage of total  $\text{VOC}_R$  (>10%-75%).

96 The potential sources of missing  $\text{VOC}_R$  include anthropogenic emissions, biogenic  
97 emissions, soil emissions, and photochemical production, etc (Yang et al., 2016b).  
98 Previous studies have reported that the missing  $\text{VOC}_R$  in forest areas was mainly from  
99 either direct emissions or photochemical oxidation of biogenic VOCs (Di Carlo et al.,  
100 2004;Hansen et al., 2014;Nakashima et al., 2014;Nölscher et al., 2016;Praplan et al.,  
101 2019). Nevertheless, the dominant source of the missing  $\text{VOC}_R$  in urban and suburban  
102 areas remains unclear or under debate.

103 Surface  $\text{O}_3$  pollution has become a major public health concern in cities worldwide  
104 (Paoletti et al., 2014;Lefohn et al., 2018). A critical issue in determining an emission  
105 control strategy for ozone pollution is to understand the relative benefits of  $\text{NO}_x$  and  
106 VOC emission controls. This is generally framed in terms of ozone precursor sensitivity,  
107 i.e., whether ozone production is  $\text{NO}_x$ -limited or VOC-limited (Kleinman,  
108 1994;Sillman et al., 1990). Nevertheless, the effect of missing VOCs on ozone  
109 precursor sensitivity has not been well understood yet. Given that the missing  $\text{VOC}_R$   
110 could potentially account for a large part of total  $\text{VOC}_R$ , clearly clarifying the role of  
111 missing  $\text{VOC}_R$  in determining ozone precursor sensitivity is an urgent need for the  
112 diagnosis of ozone sensitivity regimes and formulation of an effective emission  
113 reduction roadmap.

114 China has become a global hot spot of ground-level ozone pollution in recent years  
115 (Lu et al., 2018;Wang et al., 2022). Pearl River Delta (PRD) remains one of the most  
116  $\text{O}_3$ -polluted regions in China (Li et al., 2022), although many control measures have  
117 been attempted. Here, we measured  $\text{R}_{\text{OH}}$  in Guangzhou, a megacity in PRD and  
118 quantified the missing  $\text{VOC}_R$ . The dominant source of the missing  $\text{VOC}_R$  and its impact  
119 on ozone precursor sensitivity were comprehensively investigated.

## 120 **2 Method**

### 121 **2.1 Overview of the measurement**

122 The field campaign was conducted from 25 September to 30 October 2018  
123 continuously at an urban site in downtown Guangzhou (113.2°E, 23°N). The sampling  
124 site is located on the ninth floor of a building on the campus of Guangzhou Institute of  
125 Geochemistry, Chinese Academy of Sciences, 25 m above the ground level. This site is  
126 primarily influenced by industrial and vehicular emissions. ROH, VOCs, NOX, O<sub>3</sub>,  
127 HONO, SO<sub>2</sub>, CO, photolysis frequencies, and meteorological factors were  
128 simultaneously measured during the measurement period.

### 129 **2.2 R<sub>OH</sub> measurement**

130 Total R<sub>OH</sub> was measured by the comparative reactivity method (CRM) (Sinha et  
131 al., 2008). The CRM system consists of three major components, namely an inlet and  
132 calibration system, a reactor, and a measuring system. Here, pyrrole (C<sub>4</sub>H<sub>5</sub>N) was used  
133 as the reference substance in CRM and its concentration was quantified by a quadrupole  
134 proton-transfer-reaction mass spectrometer (PTR-MS) (Ionicon Analytik GmbH,  
135 Innsbruck, Austria). The CRM system was calibrated by propane, propene, toluene  
136 standards and 16 VOC mixed standard (acetaldehyde, methanol, ethanol, isoprene,  
137 acetone, acetonitrile, methyl vinyl ketone, methyl ethyl ketone, benzene, toluene, o-  
138 xylene,  $\alpha$ -pinene, 1,2,4-trimethylbenzene, phenol, m-cresol, and naphthalene).  
139 Measured and calculated R<sub>OH</sub> agreed well within 15% for all calibrations. The R<sub>OH</sub>  
140 measurement by the CRM method is interfered from ambient nitric oxide (NO), which  
141 produces additional OH radicals via the reaction of HO<sub>2</sub> radicals with NO (Sinha et al.,  
142 2008). To correct this interference, a series of experiments were conducted by  
143 introducing different levels of NO (0–160 ppb) and given amounts of VOC into the  
144 CRM reactor. A correction curve was acquired from these NO interference experiments,  
145 which can be used to correct the R<sub>OH</sub> thanks to the simultaneous measurement of

146 ambient NO concentrations (Supplementary information S1; Fig. S1). The detection  
147 limits of the CRM method were around  $2.5 \text{ s}^{-1}$ , and the total uncertainty was estimated  
148 to be about 15%. The CRM method has been successfully applied to measure OH  
149 reactivity in urban areas with high NO<sub>x</sub> levels in previous studies (Dolgorouky et al.,  
150 2012; Yang et al., 2017; Hansen et al., 2015). The intercomparison between the CRM  
151 method and pump-probe technique indicates that the CRM method can be used under  
152 high-NO<sub>x</sub> conditions (NO<sub>x</sub>>10 ppb) if a NO<sub>x</sub>-dependent correction is applied (Hansen  
153 et al., 2015).

### 154 2.3 VOCs measurements

155 Nonmethane hydrocarbons (NMHCs) were measured using a gas chromatograph–  
156 mass spectrometer/flame ionization detector (GC–MS/FID) system coupled with a  
157 cryogen-free preconcentration device (Wang et al., 2014). The system contains two-  
158 channel sampling and GC column separation, which is able to measure C<sub>2</sub>–C<sub>5</sub>  
159 hydrocarbons with the FID in one channel and measure C<sub>5</sub>–C<sub>12</sub> hydrocarbons using  
160 MS detector in the other channel. After removal of water vapor, VOCs were trapped at  
161  $-155 \text{ }^{\circ}\text{C}$  in a deactivated quartz capillary column (15 cm×0.53 mm ID) and a Porous  
162 Layer Open Tubular (PLOT) capillary column (15 cm×0.53 mm ID) for the MS channel  
163 and the FID channel, respectively. The system was calibrated weekly by TO-15 (Air  
164 Environmental Inc., USA) and PAMS gas standards (Spectra Gases Inc., USA).  
165 Detection limits for various compounds were in the range of 0.002–0.070 ppbv. A total  
166 of 56 NMHCs species were measured (**Table S1**). The time resolution of the  
167 measurement was 1 h. The uncertainties of VOC measurements by GC–MS/FID are in  
168 the range of 15 %–20 %. More details of this method can be found in previous studies  
169 (Wang et al., 2014; Yuan et al., 2012).

170 An online proton-transfer-reaction time-of-flight mass spectrometer (PTR-ToF-  
171 MS) (Icon Analytic GmbH, Innsbruck, Austria) with H<sub>3</sub>O<sup>+</sup> and NO<sup>+</sup> ion sources was  
172 also used to measure VOCs. During the campaign, the PTR-ToF-MS automatically  
173 switched between H<sub>3</sub>O<sup>+</sup> and NO<sup>+</sup> chemistry every 10–20 min. The H<sub>3</sub>O<sup>+</sup> mode was

174 used to measure OVOCs and aromatics while the  $\text{NO}^+$  model was used to measure  
175 alkanes with more carbons (C8-C20). When running in the  $\text{H}_3\text{O}^+$  ionization mode, the  
176 drift tube was at a temperature of 50 °C, a pressure of 3.8 mbar, and a voltage of 920  
177 V, leading to an operating E/N (E is the electric field, and N is the number density of  
178 the gas in the drift tube) ratio of 120 Td. When running in the  $\text{NO}^+$  ionization mode, the  
179 drift tube was at a temperature of 50 °C, a pressure of 3.8 mbar, and a voltage of 470  
180 V, leading to an operating E/N ratio of 60 Td. PTR-ToF-MS technique is capable of  
181 measuring oxygenated VOCs (OVOCs) and higher alkanes that GC-MS/FID cannot  
182 measure (Wu et al., 2020; Wang et al., 2020a). The time resolution of PTR-ToF-MS  
183 measurements was 10 s. A total of 31 VOCs were calibrated using either gas or liquid  
184 standards (Table S2). For other measured VOCs, we used the method proposed by  
185 Sekimoto et al. (2017) to determine the relationship between VOC sensitivity and  
186 kinetic rate constants for proton transfer reactions of  $\text{H}_3\text{O}^+$  with VOCs. The fitted line  
187 was used to determine the concentrations of those uncalibrated species. The  
188 uncertainties of the concentrations for uncalibrated species were about 50 % (Sekimoto  
189 et al., 2017). By this method, PTR-ToF-MS can additionally measure 128 VOCs which  
190 were included in the analysis of this study. The detailed information for this method can  
191 be found in Wu et al. (2020) and all VOC species measured by PTR-ToF-MS were  
192 provided in table S4 of that article. The PTR-ToF-MS is capable of measuring  
193 additional VOC species that GC-MS/FID cannot measure including alkanes with more  
194 carbons (C12-C20) and OVOCs including aldehydes, ketones, carboxylic acids,  
195 alcohols, and nitrophenols. Formaldehyde (HCHO) was measured by a custom-built  
196 instrument based on the Hantzsch reaction and absorption photometry (Xu et al., 2022).

## 197 **2.4 Other measurements**

198 Nitrous acid (HONO) was measured by a custom-built LOPAP (Long Path  
199 Absorption Photometer) based on wet chemical sampling and photometric detection  
200 (Yu et al., 2022). The uncertainty of the measurement was 8 %.  $\text{NO}_x$ ,  $\text{O}_3$ ,  $\text{SO}_2$ , and CO  
201 were measured by  $\text{NO}_x$  analyzer (Thermo Scientific, Model 42i),  $\text{O}_3$  analyzer (Thermo  
202 Scientific, Model 49i),  $\text{SO}_2$  analyzer (Thermo Scientific, Model 43i), and CO analyzer



203 (Thermo Scientific, Model 48i), respectively. The meteorological data, including  
204 temperature (T), relative humidity (RH) and wind speed and direction (WS, WD) were  
205 recorded by Vantage Pro2 Weather Station (Davis Instruments Inc., Vantage Pro2) with  
206 a time resolution of 1 min. Photolysis frequencies of O<sub>3</sub>, NO<sub>2</sub>, HONO, H<sub>2</sub>O<sub>2</sub>, HCHO,  
207 and NO<sub>3</sub> were measured by a spectrometer (Focused Photonics Inc., PFS-100) (Shetter  
208 and Müller, 1999; Wang et al., 2019).

## 209 **2.5 Multiple linear regression**

210 The Multiple Linear Regression (MLR) has been successfully applied to quantify  
211 the sources of air pollutants (Li et al., 2019; Yang et al., 2016a). In this study, a tracer-  
212 based MLR analysis was used to decouple the individual contributions of  
213 anthropogenic emissions, secondary production, biogenic emissions and background  
214 level to missing VOC<sub>R</sub>, as shown in Eq. (4).

$$215 \text{Missing VOC}_R = a\Delta\text{CO} + b[\text{O}_X] + c[\text{isoprene}_{\text{initial}}] + C_{\text{background}} \quad (4)$$

216 where O<sub>X</sub> is defined as O<sub>3</sub>+NO<sub>2</sub>. ΔCO, [O<sub>X</sub>] and [isoprene<sub>initial</sub>] are concentrations  
217 of tracers for anthropogenic emissions, secondary production and biogenic emissions,  
218 respectively. ΔCO is the relative change between ambient CO and background CO of  
219 150 ppb (Wang et al., 2020a). [isoprene<sub>initial</sub>] represents the initial concentration of  
220 isoprene from biogenic emissions that has not undergone any photochemical reactions,  
221 which is calculated from observed isoprene and its photochemical products methyl  
222 vinyl ketone (MVK) and methacrolein (MACR) (Xie et al., 2008). C<sub>background</sub>  
223 indicates the background level of missing VOC<sub>R</sub>. a, b, c and C<sub>background</sub> are fitted  
224 coefficients by the multiple linear regression.

## 225 **2.6 Observation-based box model**

226 A zero-dimensional box model coupled with the Master Chemical Mechanism  
227 (MCM) v3.3.1 chemical mechanism (Jenkin et al., 2003) was used to simulate the  
228 photochemical production of RO<sub>X</sub> (RO<sub>X</sub>=OH+HO<sub>2</sub>+RO<sub>2</sub>) radicals and O<sub>3</sub> during the  
229 field campaign. The model was constrained by the observations of meteorological

230 parameters, photolysis frequencies, VOCs, NO, NO<sub>2</sub>, O<sub>3</sub>, CO, SO<sub>2</sub>, and HONO. The  
 231 model runs were performed in a time-dependent mode with a time resolution of 1 hour  
 232 and a spin-up of four days. A 24-h lifetime was introduced for all simulated species,  
 233 including secondary species and radicals, to approximately simulate dry deposition and  
 234 other losses of these species (Lu et al., 2013; Wang et al., 2020b). Sensitivity tests show  
 235 that this assumed physical loss lifetime has a relatively small influence on RO<sub>x</sub> radicals  
 236 and ozone production rates.

237 Measured OVOCs such as HCHO, acetaldehyde and acetone were constrained in  
 238 the model and unmeasured OVOCs were simulated according to the photochemical  
 239 oxidation of NMHCs by OH radicals. RO<sub>2</sub>, HO<sub>2</sub> and OH radicals were simulated by the  
 240 box model to calculate the net O<sub>3</sub> production rate (P(O<sub>3</sub>)) and O<sub>3</sub> loss rate (L(O<sub>3</sub>)) as  
 241 shown in Equations (5) and (6) as derived by Mihelcic et al. (2003)

$$242 \quad P(O_3) = k_{HO_2+NO}[HO_2][NO] + \sum_i(k_{RO_2+NO}^i[RO_2^i][NO]) - k_{OH+NO_2}[OH][NO_2] - L(O_3)$$

243 (5)

$$244 \quad L(O_3) = (\theta j(O^1D) + k_{OH+O_3}[OH] + k_{HO_2+O_3}[HO_2] + \sum_j(k_{alkene+O_3}^j[alkene^j])[O_3]$$

245 (6)

246 where  $\theta$  is the fraction of O<sup>1</sup>D from ozone photolysis that reacts with water vapor, and  
 247  $i$  and  $j$  represent the number of species of RO<sub>2</sub> and alkenes, respectively.

248 The box model was used to evaluate the impact of missing VOC<sub>R</sub> on the O<sub>3</sub>  
 249 production rate. In the base scenario, the box model was constrained by all measured  
 250 inorganic and organic gases but the missing VOC<sub>R</sub> was not considered. To consider the  
 251 missing VOC<sub>R</sub> in the box model, we additionally increased the concentration of  
 252 NMHCs to exactly compensate for the missing VOC<sub>R</sub> by multiplying a factor, on the  
 253 basis of measured NMHC concentrations. We simulated four scenarios by increasing  
 254 the concentration of: (1) n-pentane, (2) ethylene, (3) toluene, (4) all measured 56  
 255 NMHCs. For the scenario of increasing all 56 NMHCs, concentrations of 56 NMHC  
 256 species were increased by multiplying the same factor. Given that the VOC<sub>R</sub> of  
 257 unconstrained secondary products increases with the increase in the concentration of  
 258 NMHCs, several attempts of different values are needed to determine the increasing

259 factor.

## 260 **3 Results and discussion**

### 261 **3.1 Quantification of missing $\text{VOC}_R$ during the campaign**

262 **Figure 1** shows the time series of measured  $\text{R}_{\text{OH}}$ , calculated  $\text{R}_{\text{OH}}$  according to all  
263 measured reactive gases, and missing  $\text{VOC}_R$  (the gap between measured and calculated  
264  $\text{R}_{\text{OH}}$ ) in Guangzhou. By using GC-MS/FID, we measured 56 NMHCs. By using PTR-  
265 ToF-MS, we measured 159 VOCs and 128 of them were difficult to be measured before.  
266 Besides the alkanes with carbons less than 12, PTR-ToF-MS can also measure alkanes  
267 with more carbons (C12–C20). With regard to OVOCs, not only common OVOC  
268 species including formaldehyde and C2-C4 carbonyls but also carbonyls with more  
269 carbons (C5–C10) and some N-containing OVOC species such as nitrophenol and  
270 methyl nitrophenol were measured by PTR-ToF-MS. Thanks to these additional  
271 measured VOCs, the measured  $\text{R}_{\text{OH}}$  was close to the calculated  $\text{R}_{\text{OH}}$  within 20% in most  
272 periods. In some periods the missing  $\text{VOC}_R$  was negative, which is probably due to the  
273 uncertainty in the measurements of  $\text{R}_{\text{OH}}$  and reactive gases. The negative missing  $\text{VOC}_R$   
274 primarily occurred in the afternoon (12:00–17:00) when the photochemistry was most  
275 active. Nevertheless, there were still some days exhibiting remarkable missing  $\text{VOC}_R$ .  
276 The days with missing  $\text{VOC}_R$  of more than 25% of total  $\text{R}_{\text{OH}}$ , namely high missing-  
277  $\text{VOC}_R$  days, are indicated by yellow background in **Fig. 1a**. The largest missing  $\text{VOC}_R$   
278 occurred on October 15<sup>th</sup>, 16<sup>th</sup>, 25<sup>th</sup> and 26<sup>th</sup>, with average values of  $16 \text{ s}^{-1}$ . During the  
279 period of October 24<sup>th</sup> to 26<sup>th</sup>, the total  $\text{R}_{\text{OH}}$  was highest and the missing  $\text{VOC}_R$  was also  
280 relatively high among all days. **Figure 1b** shows the contribution of different species  
281 classifications to total  $\text{R}_{\text{OH}}$  during high missing- $\text{VOC}_R$  days. Inorganic species, NMHCs  
282 and OVOCs account for 34%, 13% and 14% of total  $\text{R}_{\text{OH}}$ , respectively, with missing  
283  $\text{VOC}_R$  accounting for 39%. The fraction of missing  $\text{VOC}_R$  (39%) during the high  
284 missing- $\text{VOC}_R$  days is comparable to measurements in Los Angeles 2010 (Griffith et  
285 al., 2016) and in Seoul 2016 (Sanchez et al., 2021).

286 We evaluated the uncertainty of the missing  $\text{VOC}_R$ . The uncertainty of the  $R_{\text{OH}}$   
287 measurement was 15%. In addition, according to reports of Jet Propulsion Laboratory  
288 (Burkholder et al., 2020), reaction rate constants used for the calculation of  $R_{\text{OH}}$  in Eq  
289 (3) have uncertainties of 5%–30%, depending on different species. We took the  
290 uncertainties in the reaction rate constants and the measurements of all reactive gases  
291 into account when calculating  $R_{\text{OH}}$ , according to error propagation. As a result, the  
292 uncertainties in the missing  $\text{VOC}_R$  are  $3.8 \text{ s}^{-1}$  and  $5.2 \text{ s}^{-1}$  for the whole measurement  
293 period and the high missing- $\text{VOC}_R$  days, respectively. The average missing  $\text{VOC}_R$   
294 during the high missing- $\text{VOC}_R$  days is  $13 \text{ s}^{-1}$ , which is significantly higher than the  
295 uncertainty of  $5.2 \text{ s}^{-1}$ , suggesting that the missing  $\text{VOC}_R$  really exists during the high  
296 missing- $\text{VOC}_R$  days.

297

### 298 **3.2 The sources of missing $\text{VOC}_R$**

299 To explore the sources of missing  $\text{VOC}_R$  during the whole measurement period,  
300 we investigated the correlation between missing  $\text{VOC}_R$  and tracers characterizing  
301 primary emissions ( $\text{CO}$ ,  $\text{NO}_X$  and NMHCs) and secondary production ( $\text{O}_X \equiv \text{O}_3 + \text{NO}_2$   
302 and formic acid). The correlation of missing  $\text{VOC}_R$  with  $\text{CO}$ , reactivity of NMHCs  
303 ( $\text{NMHC}_R$ ) and  $\text{NO}_X$  is moderate, with correlation coefficient ( $R$ ) in the range of 0.47–  
304 0.56 (**Fig. 2a and b, and Fig. S2**) while there is no significant correlation of missing  
305  $\text{VOC}_R$  with  $\text{O}_X$  and formic acid (**Fig. 2c and Fig. S2**). Furthermore, there is no  
306 significant correlation between missing  $\text{VOC}_R$  and acetonitrile which is a tracer of  
307 biomass burning (de Gouw et al., 2003; Wang et al., 2007) (**Fig. S2**), indicating that  
308 biomass burning was not a major contributor to missing  $\text{VOC}_R$  during this campaign.  
309 In terms of the diurnal variation, the missing  $\text{VOC}_R$  was higher in the morning (7:00–  
310 10:00) and evening (18:00–22:00) when the anthropogenic emissions, especially  
311 vehicle exhaust were intensive, and was lower in the afternoon when the  
312 photochemistry was most active (**Fig. 2d**). The diurnal profile of missing  $\text{VOC}_R$  was  
313 similar to those of  $\text{CO}$ ,  $\text{NO}_X$  and  $\text{NMHC}_R$ . In contrast, the diurnal profiles of secondary

314 species including O<sub>x</sub>, formic acid and acetic acid, which peaked in the afternoon,  
315 evidently differ from the diurnal profile of missing VOC<sub>R</sub> (**Fig. S3**). Further, we  
316 investigated the influence of air mass aging on missing VOC<sub>R</sub>. The ratio of ethylbenzene  
317 to m,p-xylene was used to characterize the degree of air mass aging (De Gouw et al.,  
318 2005; Yuan et al., 2013). A higher ratio of ethylbenzene to m,p-xylene corresponds to a  
319 higher degree of air mass aging as the m,p-xylene has a larger reaction rate constant  
320 ( $18.9 \times 10^{-12} \text{ cm}^3 \text{ molecule}^{-1} \text{ s}^{-1}$ ) than ethylbenzene ( $7.0 \times 10^{-12} \text{ cm}^3 \text{ molecule}^{-1} \text{ s}^{-1}$ ) when  
321 reacting with the major oxidant - OH radicals. As shown in **Fig. 2e**, missing VOC<sub>R</sub>  
322 decreases with the ratio of ethylbenzene to m,p-xylene. Given that secondary  
323 production generally increased with air mass aging, this result further demonstrates that  
324 missing VOC<sub>R</sub> was not caused by enhanced secondary production.

325 During the high missing- VOC<sub>R</sub> days, the correlation coefficient for missing VOC<sub>R</sub>  
326 versus CO is 0.76 (**Fig. 3a**), which is higher than that in the whole measurement period  
327 (0.56) shown in **Fig. 2a**. We then quantify the sources of missing VOC<sub>R</sub> during the high  
328 missing- VOC<sub>R</sub> days by applying MLR. The fitted coefficients are as follows: a is 0.031  
329  $\text{s}^{-1} \text{ ppb}^{-1}$ , b is 0.012  $\text{s}^{-1} \text{ ppb}^{-1}$ , c is 1.8  $\text{s}^{-1} \text{ ppb}^{-1}$  and  $C_{\text{background}}$  is 1.3  $\text{s}^{-1}$ . The coefficient  
330 of determination ( $R^2$ ) for the MLR is 0.68. As shown in **Fig. 3b**, anthropogenic  
331 emissions were the largest contributor to missing VOC<sub>R</sub>, accounting for 70% of missing  
332 VOC<sub>R</sub>. Secondary production, biogenic emissions and background contribution played  
333 a minor role in missing VOC<sub>R</sub> (13%, 7%, 10%, respectively). The parametric  
334 relationship between missing VOC<sub>R</sub> and relevant tracers established by MLR provides  
335 a valid approach to estimate the missing VOC<sub>R</sub> according to readily available gases  
336 including CO, O<sub>x</sub> and isoprene.

337 Although anthropogenic emissions are identified to be the major source of missing  
338 VOC<sub>R</sub>, which species dominantly contribute to the missing VOC<sub>R</sub> remains unclear. A  
339 potential source is the unmeasured branched alkenes for their high reactivity, previously  
340 observed from vehicle exhaust (Nakashima et al., 2010) and gasoline evaporation  
341 emissions (Wu et al., 2015). Another possible source is emitted OVOCs with a more  
342 complex functional group that cannot be accurately measured. In addition, directly

343 emitted semi-volatile and intermediate volatility organic compounds are also possible  
344 sources of missing VOC<sub>R</sub> (Stewart et al., 2021).

### 345 **3.3 The impact of missing VOC<sub>R</sub> on O<sub>3</sub> sensitivity regimes**

346 The reaction of OH with VOCs is key to the propagation and amplification of OH  
347 radicals, thus determining the ozone production rate (Tonnesen and Dennis, 2000). The  
348 box model was used to evaluate the impact of missing VOC<sub>R</sub> on the O<sub>3</sub> production rate  
349 during high missing-VOC<sub>R</sub> days. The setting of model simulations for different  
350 scenarios are depicted in Section 2.6. Under the base scenario, on average the measured  
351 VOC<sub>R</sub> of n-pentane, ethylene, toluene and all 56 NMHCs are 0.14 s<sup>-1</sup>, 0.53 s<sup>-1</sup>, 0.60 s<sup>-1</sup>  
352 and 4.6 s<sup>-1</sup> respectively. To consider the missing VOC<sub>R</sub> (on average of 13 s<sup>-1</sup>) in the  
353 model, four scenarios were simulated by additionally increasing n-pentane, ethylene,  
354 toluene and 56 NMHCs by a factor of 70, 16, 13.3 and 1.9, respectively. These  
355 increasing factors led to an additional increase in VOC<sub>R</sub> of both NMHCs and  
356 unconstrained secondary products, which exactly compensated for the missing VOC<sub>R</sub>.  
357 **Figure 4** shows the simulated P(O<sub>3</sub>) for the base scenario and the scenarios considering  
358 missing VOC<sub>R</sub>. The daytime average P(O<sub>3</sub>) under the scenarios considering missing  
359 VOC<sub>R</sub> is a factor of 1.5–4.5 for the results under the base scenario. The difference in  
360 added species has a large effect on P(O<sub>3</sub>). Adding toluene causes a larger increase in  
361 P(O<sub>3</sub>) than adding n-pentane or ethene, as toluene has a stronger ability to amplify the  
362 production of radicals.

363 O<sub>3</sub> precursor sensitivity depends on the dominant loss pathways of RO<sub>X</sub> radicals  
364 (RO<sub>X</sub>=OH+HO<sub>2</sub>+RO<sub>2</sub>). O<sub>3</sub> production is NO<sub>X</sub>-limited if the self-reaction of peroxy  
365 radicals (HO<sub>2</sub> and RO<sub>2</sub>) dominates the RO<sub>X</sub> sink, and VOC-limited if the reaction of  
366 NO<sub>2</sub> with OH dominates (Kleinman et al., 1997; Kleinman et al., 2001). Accordingly,  
367 the ratio of RO<sub>X</sub> sink induced by OH+NO<sub>2</sub> reaction to the total rate of the two RO<sub>X</sub>  
368 sinks, i.e., L<sub>N</sub>/Q, is used to identify O<sub>3</sub> sensitivity regimes. O<sub>3</sub> production is NO<sub>X</sub>-  
369 limited if L<sub>N</sub>/Q is lower than 0.5, otherwise, it is VOC-limited (Kleinman et al., 1997).

$$370 \quad L_N/Q = \frac{k_{OH+NO_2}[OH][NO_2]}{k_{HO_2+RO_2}[HO_2][RO_2]+k_{HO_2+HO_2}[HO_2][HO_2]+k_{OH+HO_2}[OH][HO_2]+k_{OH+NO_2}[OH][NO_2]}$$

371

(7)

372 As shown in **Fig. 5a**, under the base scenario,  $L_N/Q$  remained at a stable and high  
373 level ( $>0.9$ ) during the daytime when photochemical production of ozone occurs,  
374 indicating  $O_3$  production was VOC-limited. Under the scenarios considering missing  
375  $VOC_R$ ,  $L_N/Q$  decreased significantly regardless of which VOC species was added,  
376 compared to the base scenario. Adding toluene caused the largest decrease in  $L_N/Q$ ,  
377 followed by adding all measured NMHC species, adding the alkane and adding the  
378 alkene. It is worth noting that adding toluene and all measured NMHC species caused  
379 the  $L_N/Q$  to be close to 0.5 in the afternoon, indicating that the  $O_3$  production shifted to  
380 transitional or  $NO_X$ -limited regimes in these scenarios. **Fig. 5b** shows the changes in  
381 radical sinks before and after considering missing  $VOC_R$ . All radical sinks including  
382 self-reactions of peroxy radicals and  $OH+NO_2$  reaction increased after considering  
383 missing  $VOC_R$ . Nevertheless, the increased proportion of the self-reactions of peroxy  
384 radicals was larger than that of  $OH+NO_2$  reaction, leading to a decrease in  $L_N/Q$  and  
385 thus a shift toward  $NO_X$ -limited regime.

386 **Figure 5c** shows the dependence of daily peak  $O_3$  concentrations on  $NO_X$   
387 concentrations, which was calculated by the box model for the base scenario and the  
388 scenario considering missing  $VOC_R$ . The  $NO_X$  concentration level corresponding to the  
389 maximum of  $O_3$  concentrations was determined. This  $NO_X$  concentration level reflects  
390 the threshold to distinguish between VOC-limited and  $NO_X$ -limited regimes. The larger  
391 threshold of  $NO_X$  represents a higher possibility of ozone production in  $NO_X$  limited  
392 regime. The threshold of  $NO_X$  for the scenario considering missing  $VOC_R$  is 46% higher  
393 than for the base scenario. Note that the uncertainty in missing  $VOC_R$  leads to 17%  
394 uncertainty in the threshold of  $NO_X$  for the scenario considering missing  $VOC_R$ . Overall,  
395 **Fig. 5** suggests that omitting the missing  $VOC_R$  will overestimate the degree of the  
396 VOC-limited regime and thus overestimate the effect of VOCs abatement in reducing  
397 ozone pollution, which in turn may mislead ozone control strategy.

### 398 **3.4 Atmospheric implications**

399 Although many previous studies have reported that photochemical production  
400 processes and biogenic emissions are important sources of missing VOC<sub>R</sub> (Lou et al.,  
401 2010;Dolgorouky et al., 2012;Yang et al., 2017;Sanchez et al., 2021;Di Carlo et al.,  
402 2004), we find that anthropogenic emissions may dominate the missing VOC<sub>R</sub> in urban  
403 regions. In zero-dimensional box models and three-dimensional chemistry-transport  
404 models, the input of VOCs emission information mainly contains well-studied simple-  
405 structure alkanes, alkenes and aromatics, while those unmeasured/unknown VOC  
406 species have been neglected. This will lead to biases in quantifying ozone production  
407 and diagnosing ozone sensitivity regimes. Our study demonstrates that the ambient  
408 measurement of R<sub>OH</sub> at urban sites can provide quantification of missing VOC<sub>R</sub>, which  
409 can be used in models to account for the missing VOC<sub>R</sub> from anthropogenic emissions.  
410 In addition, the parametric equation of missing VOC<sub>R</sub> derived from MLR method (Eq  
411 (4)) here can be used to estimate missing VOC<sub>R</sub> according to measurements of CO, O<sub>x</sub>  
412 and isoprene. Further study should try to parse the specific sources of the missing VOC<sub>R</sub>,  
413 e.g., whether the missing VOC<sub>R</sub> is from intermediate-volatility and semivolatile organic  
414 compounds emitted from vehicles or whether it is from some other sources.  
415 Furthermore, future studies can focus on direct measurements of missing VOC<sub>R</sub> for  
416 various emission sources to develop a comprehensive emission inventory of missing  
417 VOC<sub>R</sub>, which will help to improve O<sub>3</sub> pollution mitigation strategies.

418

#### 419 **Data availability**

420 The observational data and model code used in this study are available from  
421 corresponding authors upon request ([byuan@jnu.edu.cn](mailto:byuan@jnu.edu.cn)).

#### 422 **Author contributions**

423 BY and WJW designed the research. WJW and BY prepared the manuscript with  
424 contributions from other authors. WJW performed data analysis with contributions



425 from HS, YFC, FXB. CYX, CQM. JPQ, SHW, WS, XMW, HLW, SRL and MS  
426 collected data

## 427 **Competing interests**

428 At least one of the (co-)authors is a member of the editorial board of Atmospheric  
429 Chemistry and Physics.

## 430 **Acknowledgement**

431 This work was supported by the National Natural Science Foundation of China (grant  
432 No. , 42121004, 42275103, 42230701, 42175135). This work was also supported by  
433 Special Fund Project for Science and Technology Innovation Strategy of Guangdong  
434 Province (Grant No.2019B121205004).

## 435 **References**

- 436 Atkinson, R.: Atmospheric chemistry of VOCs and NO<sub>x</sub>, *Atmos. Environ.*, 34, 2063-2101, 2000.
- 437 Atkinson, R., and Arey, J.: Atmospheric degradation of volatile organic compounds, *Chemical*  
438 *reviews*, 103, 4605-4638, 2003.
- 439 Burkholder, J., Sander, S., Abbatt, J., Barker, J., Cappa, C., Crouse, J., Dibble, T., Huie, R., Kolb,  
440 C., and Kurylo, M.: Chemical kinetics and photochemical data for use in atmospheric studies;  
441 evaluation number 19, Pasadena, CA: Jet Propulsion Laboratory, National Aeronautics and  
442 Space ..., 2020.
- 443 De Gouw, J., Middlebrook, A., Warneke, C., Goldan, P., Kuster, W., Roberts, J., Fehsenfeld, F.,  
444 Worsnop, D., Canagaratna, M., and Pszenny, A.: Budget of organic carbon in a polluted  
445 atmosphere: Results from the New England Air Quality Study in 2002, *J. Geophys. Res.-Atmos.*,  
446 110, 2005.
- 447 de Gouw, J. A., Warneke, C., Parrish, D. D., Holloway, J. S., Trainer, M., and Fehsenfeld, F. C.:  
448 Emission sources and ocean uptake of acetonitrile (CH<sub>3</sub>CN) in the atmosphere, *J. Geophys.*  
449 *Res.-Atmos.*, 108, <https://doi.org/10.1029/2002JD002897>, 2003.
- 450 Di Carlo, P., Brune, W. H., Martinez, M., Harder, H., Leshner, R., Ren, X. R., Thornberry, T., Carroll,  
451 M. A., Young, V., Shepson, P. B., Riemer, D., Apel, E., and Campbell, C.: Missing OH  
452 reactivity in a forest: Evidence for unknown reactive biogenic VOCs, *Science*, 304, 722-725,  
453 10.1126/science.1094392, 2004.
- 454 Dolgorouky, C., Gros, V., Sarda-Esteve, R., Sinha, V., Williams, J., Marchand, N., Sauvage, S.,  
455 Poulain, L., Sciare, J., and Bonsang, B.: Total OH reactivity measurements in Paris during the  
456 2010 MEGAPOLI winter campaign, *Atmos. Chem. Phys.*, 12, 9593-9612, 10.5194/acp-12-  
457 9593-2012, 2012.
- 458 Fuchs, H., Tan, Z., Lu, K., Bohn, B., Broch, S., Brown, S. S., Dong, H., Gomm, S., Häsel, R., He,  
459 L., Hofzumahaus, A., Holland, F., Li, X., Liu, Y., Lu, S., Min, K. E., Rohrer, F., Shao, M.,  
460 Wang, B., Wang, M., Wu, Y., Zeng, L., Zhang, Y., Wahner, A., and Zhang, Y.: OH reactivity

461 at a rural site (Wangdu) in the North China Plain: contributions from OH reactants and  
462 experimental OH budget, *Atmos. Chem. Phys.*, 17, 645-661, 10.5194/acp-17-645-2017, 2017.

463 Goldstein, A. H., and Galbally, I. E.: Known and unexplored organic constituents in the earth's  
464 atmosphere, *Environ. Sci. Technol.*, 41, 1514-1521, 2007.

465 Griffith, S. M., Hansen, R., Dusanter, S., Michoud, V., Gilman, J., Kuster, W., Veres, P., Graus, M.,  
466 de Gouw, J., and Roberts, J.: Measurements of hydroxyl and hydroperoxy radicals during  
467 CalNex-LA: Model comparisons and radical budgets, *J. Geophys. Res.-Atmos.*, 121, 4211-4232,  
468 2016.

469 Hansen, R. F., Griffith, S. M., Dusanter, S., Rickly, P. S., Stevens, P. S., Bertman, S. B., Carroll, M.  
470 A., Erickson, M. H., Flynn, J. H., Grossberg, N., Jobson, B. T., Lefer, B. L., and Wallace, H.  
471 W.: Measurements of total hydroxyl radical reactivity during CABINEX 2009 &ndash; Part 1:  
472 field measurements, *Atmos. Chem. Phys.*, 14, 2923-2937, 10.5194/acp-14-2923-2014, 2014.

473 Hansen, R. F., Blocquet, M., Schoemaeker, C., Léonardis, T., Locoge, N., Fittschen, C., Hanoune,  
474 B., Stevens, P. S., Sinha, V., and Dusanter, S.: Intercomparison of the comparative reactivity  
475 method (CRM) and pump-probe technique for measuring total OH reactivity in an urban  
476 environment, *Atmos. Meas. Tech.*, 8, 4243-4264, 10.5194/amt-8-4243-2015, 2015.

477 Jenkin, M. E., Saunders, S. M., Wagner, V., and Pilling, M. J.: Protocol for the development of the  
478 Master Chemical Mechanism, MCM v3 (Part B): tropospheric degradation of aromatic volatile  
479 organic compounds, *Atmos. Chem. Phys.*, 3, 181-193, 10.5194/acp-3-181-2003, 2003.

480 Kleinman, L. I.: Low and high NO<sub>x</sub> tropospheric photochemistry, *J. Geophys. Res.-Atmos.*, 99,  
481 16831-16838, 1994.

482 Kleinman, L. I., Daum, P. H., Lee, J. H., Lee, Y. N., Nunnermacker, L. J., Springston, S. R.,  
483 Newman, L., Weinstein-Lloyd, J., and Sillman, S.: Dependence of ozone production on NO and  
484 hydrocarbons in the troposphere, *Geophys. Res. Lett.*, 24, 2299-2302, 1997.

485 Kleinman, L. I., Daum, P. H., Lee, Y. N., Nunnermacker, L. J., Springston, S. R., Weinstein-Lloyd,  
486 J., and Rudolph, J.: Sensitivity of ozone production rate to ozone precursors, *Geophys. Res.*  
487 *Lett.*, 28, 2903-2906, 2001.

488 Kovacs, T., Brune, W., Harder, H., Martinez, M., Simpas, J., Frost, G., Williams, E., Jobson, T.,  
489 Stroud, C., and Young, V.: Direct measurements of urban OH reactivity during Nashville SOS  
490 in summer 1999, *Journal of Environmental Monitoring*, 5, 68-74, 2003.

491 Lefohn, A. S., Malley, C. S., Smith, L., Wells, B., Hazucha, M., Simon, H., Naik, V., Mills, G.,  
492 Schultz, M. G., and Paoletti, E.: Tropospheric ozone assessment report: Global ozone metrics  
493 for climate change, human health, and crop/ecosystem research, *Elem. Sci. Anth.*, 6, 2018.

494 Li, K., Jacob, D. J., Liao, H., Shen, L., Zhang, Q., and Bates, K. H.: Anthropogenic drivers of 2013–  
495 2017 trends in summer surface ozone in China, *Proc. National Acad. Sci.*, 116, 422-427, 2019.

496 Li, X.-B., Yuan, B., Parrish, D. D., Chen, D., Song, Y., Yang, S., Liu, Z., and Shao, M.: Long-term  
497 trend of ozone in southern China reveals future mitigation strategy for air pollution, *Atmos.*  
498 *Environ.*, 269, 118869, 2022.

499 Lou, S., Holland, F., Rohrer, F., Lu, K., Bohn, B., Brauers, T., Chang, C., Fuchs, H., Häseler, R.,  
500 and Kita, K.: Atmospheric OH reactivities in the Pearl River Delta–China in summer 2006:  
501 measurement and model results, *Atmos. Chem. Phys.*, 10, 11243-11260, 2010.

502 Lu, K. D., Hofzumahaus, A., Holland, F., Bohn, B., Brauers, T., Fuchs, H., Hu, M., Haseler, R.,  
503 Kita, K., Kondo, Y., Li, X., Lou, S. R., Oebel, A., Shao, M., Zeng, L. M., Wahner, A., Zhu, T.,  
504 Zhang, Y. H., and Rohrer, F.: Missing OH source in a suburban environment near Beijing:

505 observed and modelled OH and HO<sub>2</sub> concentrations in summer 2006, *Atmospheric Chemistry*  
506 *and Physics*, 13, 1057-1080, 10.5194/acp-13-1057-2013, 2013.

507 Lu, X., Hong, J. Y., Zhang, L., Cooper, O. R., Schultz, M. G., Xu, X. B., Wang, T., Gao, M., Zhao,  
508 Y. H., and Zhang, Y. H.: Severe Surface Ozone Pollution in China: A Global Perspective,  
509 *Environ. Sci. Technol. Lett.*, 5, 487-494, 10.1021/acs.estlett.8b00366, 2018.

510 Mihelcic, D., Holland, F., Hofzumahaus, A., Hoppe, L., Konrad, S., Müsgen, P., Pätz, H. W.,  
511 Schäfer, H. J., Schmitz, T., and Volz-Thomas, A.: Peroxy radicals during BERLIOZ at  
512 Pabstthum: Measurements, radical budgets and ozone production, *J. Geophys. Res.-Atmos.*, 108,  
513 2003.

514 Monks, P. S., Archibald, A. T., Colette, A., Cooper, O., Coyle, M., Derwent, R., Fowler, D., Granier,  
515 C., Law, K. S., Mills, G. E., Stevenson, D. S., Tarasova, O., Thouret, V., von Schneidemesser,  
516 E., Sommariva, R., Wild, O., and Williams, M. L.: Tropospheric ozone and its precursors from  
517 the urban to the global scale from air quality to short-lived climate forcer, *Atmos. Chem. Phys.*,  
518 15, 8889-8973, 10.5194/acp-15-8889-2015, 2015.

519 Nakashima, Y., Kamei, N., Kobayashi, S., and Kajii, Y.: Total OH reactivity and VOC analyses for  
520 gasoline vehicular exhaust with a chassis dynamometer, *Atmos. Environ.*, 44, 468-475,  
521 <https://doi.org/10.1016/j.atmosenv.2009.11.006>, 2010.

522 Nakashima, Y., Kato, S., Greenberg, J., Harley, P., Karl, T., Turnipseed, A., Apel, E., Guenther, A.,  
523 Smith, J., and Kajii, Y.: Total OH reactivity measurements in ambient air in a southern Rocky  
524 mountain ponderosa pine forest during BEACHON-SRM08 summer campaign, *Atmos.*  
525 *Environ.*, 85, 1-8, <https://doi.org/10.1016/j.atmosenv.2013.11.042>, 2014.

526 Nölscher, A. C., Yañez-Serrano, A. M., Wolff, S., de Araujo, A. C., Lavrič, J. V., Kesselmeier, J.,  
527 and Williams, J.: Unexpected seasonality in quantity and composition of Amazon rainforest air  
528 reactivity, *Nature Communications*, 7, 10383, 10.1038/ncomms10383, 2016.

529 Paoletti, E., De Marco, A., Beddows, D. C., Harrison, R. M., and Manning, W. J.: Ozone levels in  
530 European and USA cities are increasing more than at rural sites, while peak values are  
531 decreasing, *Environmental Pollution*, 192, 295-299, 2014.

532 Praplan, A. P., Tykka, T., Chen, D., Boy, M., Taipale, D., Vakkari, V., Zhou, P. T., Petaja, T., and  
533 Hellen, H.: Long-term total OH reactivity measurements in a boreal forest, *Atmos. Chem. Phys.*,  
534 19, 14431-14453, 10.5194/acp-19-14431-2019, 2019.

535 Sadanaga, Y., Yoshino, A., Kato, S., and Kajii, Y.: Measurements of OH reactivity and  
536 photochemical ozone production in the urban atmosphere, *Environ. Sci. Technol.*, 39, 8847-  
537 8852, 2005.

538 Sanchez, D., Seco, R., Gu, D., Guenther, A., Mak, J., Lee, Y., Kim, D., Ahn, J., Blake, D., Herndon,  
539 S., Jeong, D., Sullivan, J. T., McGee, T., Park, R., and Kim, S.: Contributions to OH reactivity  
540 from unexplored volatile organic compounds measured by PTR-ToF-MS – a case study in a  
541 suburban forest of the Seoul metropolitan area during the Korea–United States Air Quality  
542 Study (KORUS-AQ) 2016, *Atmos. Chem. Phys.*, 21, 6331-6345, 10.5194/acp-21-6331-2021,  
543 2021.

544 Sekimoto, K., Li, S.-M., Yuan, B., Koss, A., Coggon, M., Warneke, C., and de Gouw, J.: Calculation  
545 of the sensitivity of proton-transfer-reaction mass spectrometry (PTR-MS) for organic trace  
546 gases using molecular properties, *International Journal of Mass Spectrometry*, 421, 71-94,  
547 [10.1016/j.ijms.2017.04.006](https://doi.org/10.1016/j.ijms.2017.04.006), 2017.

548 Shetter, R. E., and Müller, M.: Photolysis frequency measurements using actinic flux  
549 spectroradiometry during the PEM-Tropics mission: Instrumentation description and some  
550 results, *J. Geophys. Res.-Atmos.*, 104, 5647-5661, <https://doi.org/10.1029/98JD01381>, 1999.

551 Shirley, T. R., Brune, W. H., Ren, X., Mao, J., Leshner, R., Cardenas, B., Volkamer, R., Molina, L.  
552 T., Molina, M. J., Lamb, B., Velasco, E., Jobson, T., and Alexander, M.: Atmospheric oxidation  
553 in the Mexico City Metropolitan Area (MCMA) during April 2003, *Atmos. Chem. Phys.*, 6,  
554 2753-2765, 10.5194/acp-6-2753-2006, 2006.

555 Sillman, S., Logan, J. A., and Wofsy, S. C.: The sensitivity of ozone to nitrogen oxides and  
556 hydrocarbons in regional ozone episodes, *J. Geophys. Res.-Atmos.*, 95, 1837-1851, 1990.

557 Sinha, V., Williams, J., Crowley, J., and Lelieveld, J.: The Comparative Reactivity Method—a new  
558 tool to measure total OH Reactivity in ambient air, *Atmos. Chem. Phys.*, 8, 2213-2227, 2008.

559 Song, K., Gong, Y., Guo, S., Lv, D., Wang, H., Wan, Z., Yu, Y., Tang, R., Li, T., Tan, R., Zhu, W.,  
560 Shen, R., and Lu, S.: Investigation of partition coefficients and fingerprints of atmospheric gas-  
561 and particle-phase intermediate volatility and semi-volatile organic compounds using pixel-  
562 based approaches, *Journal of Chromatography A*, 1665, 462808,  
563 <https://doi.org/10.1016/j.chroma.2022.462808>, 2022.

564 Stewart, G. J., Nelson, B. S., Acton, W. J. F., Vaughan, A. R., Farren, N. J., Hopkins, J. R., Ward,  
565 M. W., Swift, S. J., Arya, R., Mondal, A., Jangirh, R., Ahlawat, S., Yadav, L., Sharma, S. K.,  
566 Yunus, S. S. M., Hewitt, C. N., Nemitz, E., Mullinger, N., Gadi, R., Sahu, L. K., Tripathi, N.,  
567 Rickard, A. R., Lee, J. D., Mandal, T. K., and Hamilton, J. F.: Emissions of intermediate-  
568 volatility and semi-volatile organic compounds from domestic fuels used in Delhi, India, *Atmos.*  
569 *Chem. Phys.*, 21, 2407-2426, 10.5194/acp-21-2407-2021, 2021.

570 Tonnesen, G. S., and Dennis, R. L.: Analysis of radical propagation efficiency to assess ozone  
571 sensitivity to hydrocarbons and NO<sub>x</sub>: 1. Local indicators of instantaneous odd oxygen  
572 production sensitivity, *J. Geophys. Res.-Atmos.*, 105, 9213-9225, 2000.

573 Wang, C., Yuan, B., Wu, C., Wang, S., Qi, J., Wang, B., Wang, Z., Hu, W., Chen, W., Ye, C., Wang,  
574 W., Sun, Y., Wang, C., Huang, S., Song, W., Wang, X., Yang, S., Zhang, S., Xu, W., Ma, N.,  
575 Zhang, Z., Jiang, B., Su, H., Cheng, Y., Wang, X., and Shao, M.: Measurements of higher  
576 alkanes using NO<sup>+</sup> chemical ionization in PTR-ToF-MS: important contributions of higher  
577 alkanes to secondary organic aerosols in China, *Atmospheric Chemistry and Physics*, 20,  
578 14123-14138, 10.5194/acp-20-14123-2020, 2020a.

579 Wang, H., Zhang, X., and Chen, Z.: Development of DNPH/HPLC method for the measurement of  
580 carbonyl compounds in the aqueous phase: applications to laboratory simulation and field  
581 measurement, *Environmental Chemistry*, 6, 389-397, <https://doi.org/10.1071/EN09057>, 2009.

582 Wang, M., Zeng, L., Lu, S., Shao, M., Liu, X., Yu, X., Chen, W., Yuan, B., Zhang, Q., and Hu, M.:  
583 Development and validation of a cryogen-free automatic gas chromatograph system (GC-  
584 MS/FID) for online measurements of volatile organic compounds, *Anal. Methods*, 6, 9424-9434,  
585 2014.

586 Wang, Q. Q., Shao, M., Liu, Y., William, K., Paul, G., Li, X. H., Liu, Y. A., and Lu, S. H.: Impact  
587 of biomass burning on urban air quality estimated by organic tracers: Guangzhou and Beijing  
588 as cases, *Atmos. Environ.*, 41, 8380-8390, 10.1016/j.atmosenv.2007.06.048, 2007.

589 Wang, W., Li, X., Shao, M., Hu, M., Zeng, L., Wu, Y., and Tan, T.: The impact of aerosols on  
590 photolysis frequencies and ozone production in Beijing during the 4-year period 2012–2015,  
591 *Atmos. Chem. Phys.*, 19, 9413-9429, 10.5194/acp-19-9413-2019, 2019.

592 Wang, W., Parrish, D. D., Li, X., Shao, M., Liu, Y., Mo, Z., Lu, S., Hu, M., Fang, X., and Wu, Y.:  
593 Exploring the drivers of the increased ozone production in Beijing in summertime during 2005–  
594 2016, *Atmos. Chem. Phys.*, 20, 15617-15633, 2020b.

595 Wang, W., Parrish, D. D., Wang, S., Bao, F., Ni, R., Li, X., Yang, S., Wang, H., Cheng, Y., and Su,  
596 H.: Long-term trend of ozone pollution in China during 2014–2020: distinct seasonal and spatial  
597 characteristics and ozone sensitivity, *Atmos. Chem. Phys.*, 22, 8935-8949, 10.5194/acp-22-  
598 8935-2022, 2022.

599 Wu, C., Wang, C., Wang, S., Wang, W., Yuan, B., Qi, J., Wang, B., Wang, H., Wang, C., and Song,  
600 W.: Measurement report: Important contributions of oxygenated compounds to emissions and  
601 chemistry of volatile organic compounds in urban air, *Atmos. Chem. Phys.*, 20, 14769-14785,  
602 2020.

603 Wu, Y., Yang, Y. D., Shao, M., and Lu, S. H.: Missing in total OH reactivity of VOCs from gasoline  
604 evaporation, *Chinese Chemical Letters*, 26, 1246-1248, 10.1016/j.ccllet.2015.05.047, 2015.

605 Xie, X., Shao, M., Liu, Y., Lu, S., Chang, C.-C., and Chen, Z.-M.: Estimate of initial isoprene  
606 contribution to ozone formation potential in Beijing, China, *Atmos. Environ.*, 42, 6000-6010,  
607 2008.

608 Xu, R., Li, X., Dong, H., Lv, D., Kim, N., Yang, S., Wang, W., Chen, J., Shao, M., and Lu, S.: Field  
609 observations and quantifications of atmospheric formaldehyde partitioning in gaseous and  
610 particulate phases, *Sci. Total Environ.*, 808, 152122, 2022.

611 Yang, Y., Liao, H., and Lou, S.: Increase in winter haze over eastern China in recent decades: Roles  
612 of variations in meteorological parameters and anthropogenic emissions, *J. Geophys. Res.-  
613 Atmos.*, 121, 13,050-013,065, <https://doi.org/10.1002/2016JD025136>, 2016a.

614 Yang, Y., Shao, M., Wang, X., Nölscher, A. C., Kessel, S., Guenther, A., and Williams, J.: Towards  
615 a quantitative understanding of total OH reactivity: A review, *Atmos. Environ.*, 134, 147-161,  
616 2016b.

617 Yang, Y., Shao, M., Keßel, S., Li, Y., Lu, K., Lu, S., Williams, J., Zhang, Y., Zeng, L., Nölscher,  
618 A. C., Wu, Y., Wang, X., and Zheng, J.: How the OH reactivity affects the ozone production  
619 efficiency: case studies in Beijing and Heshan, China, *Atmos. Chem. Phys.*, 17, 7127-7142,  
620 10.5194/acp-17-7127-2017, 2017.

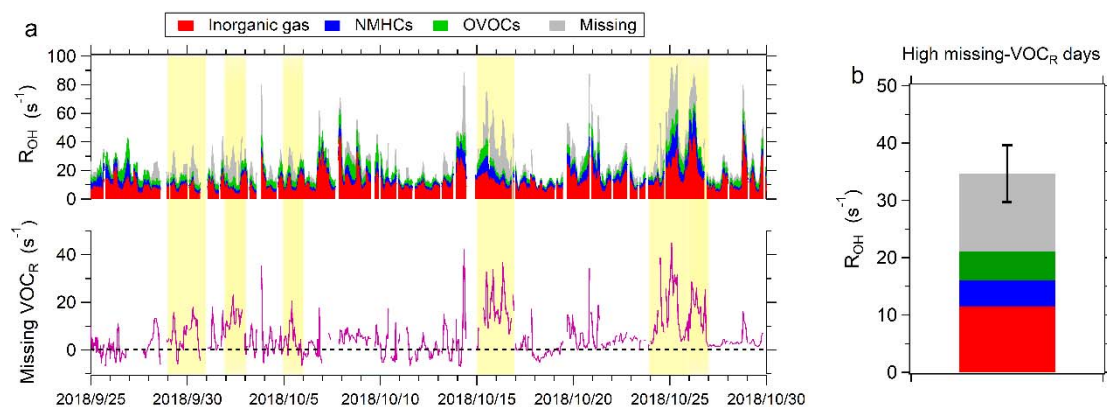
621 Yoshino, A., Sadanaga, Y., Watanabe, K., Kato, S., Miyakawa, Y., Matsumoto, J., and Kajii, Y.:  
622 Measurement of total OH reactivity by laser-induced pump and probe technique—  
623 comprehensive observations in the urban atmosphere of Tokyo, *Atmos. Environ.*, 40, 7869-  
624 7881, <https://doi.org/10.1016/j.atmosenv.2006.07.023>, 2006.

625 Yu, Y., Cheng, P., Li, H., Yang, W., Han, B., Song, W., Hu, W., Wang, X., Yuan, B., Shao, M.,  
626 Huang, Z., Li, Z., Zheng, J., Wang, H., and Yu, X.: Budget of nitrous acid (HONO) at an urban  
627 site in the fall season of Guangzhou, China, *Atmos. Chem. Phys.*, 22, 8951-8971, 10.5194/acp-  
628 22-8951-2022, 2022.

629 Yuan, B., Chen, W., Shao, M., Wang, M., Lu, S., Wang, B., Liu, Y., Chang, C.-C., and Wang, B.:  
630 Measurements of ambient hydrocarbons and carbonyls in the Pearl River Delta (PRD), China,  
631 *Atmos. Res.*, 116, 93-104, 2012.

632 Yuan, B., Hu, W., Shao, M., Wang, M., Chen, W., Lu, S., Zeng, L., and Hu, M.: VOC emissions,  
633 evolutions and contributions to SOA formation at a receptor site in eastern China, *Atmos. Chem.  
634 Phys.*, 13, 8815-8832, 2013.

635 Yuan, B., Koss, A. R., Warneke, C., Coggon, M., Sekimoto, K., and de Gouw, J. A.: Proton-  
636 Transfer-Reaction Mass Spectrometry: Applications in Atmospheric Sciences, *Chemical*  
637 *Reviews*, 117, 13187-13229, 10.1021/acs.chemrev.7b00325, 2017.  
638



640

641 **Figure 1. The level of missing  $VOC_R$  during the measurements in Guangzhou. (a)**642 Time series of measured  $R_{OH}$  and calculated  $R_{OH}$  from all measured reactive gases in643 Guangzhou. Yellow background represents the high missing- $VOC_R$  days with missing644  $VOC_R$  accounting for more than 30% of total  $R_{OH}$ . (b) Contributions of different645 compositions to  $R_{OH}$  in high missing- $VOC_R$  days. The error bar represents standard646 deviation of missing  $VOC_R$ .

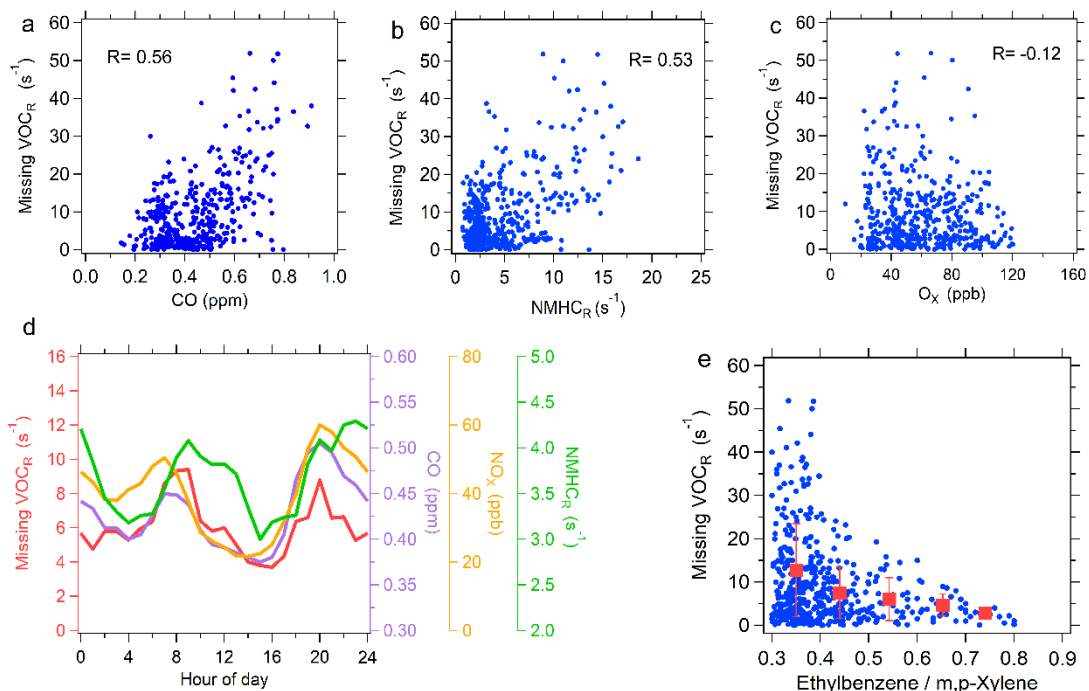
647

648

649

650

651



652

653 **Figure 2. Correlation of missing VOC<sub>R</sub> with major tracers during the whole**

654 **measurement period. (a-c) Correlation of missing VOC<sub>R</sub> with CO, OH reactivity of**

655 **NMHCs (NMHC<sub>R</sub>) and O<sub>X</sub>. Each point represents hourly data. (d) Diurnal variations**

656 **in missing VOC<sub>R</sub>, CO, NO<sub>X</sub> and NMHCs. (e) The dependence of missing VOC<sub>R</sub> on**

657 **ethylbenzene to m, p-xylene ratio. The red squares indicate the mean values of missing**

658 **VOCR in different ranges of ethylbenzene/m,p-xylene with classification width of 0.1,**

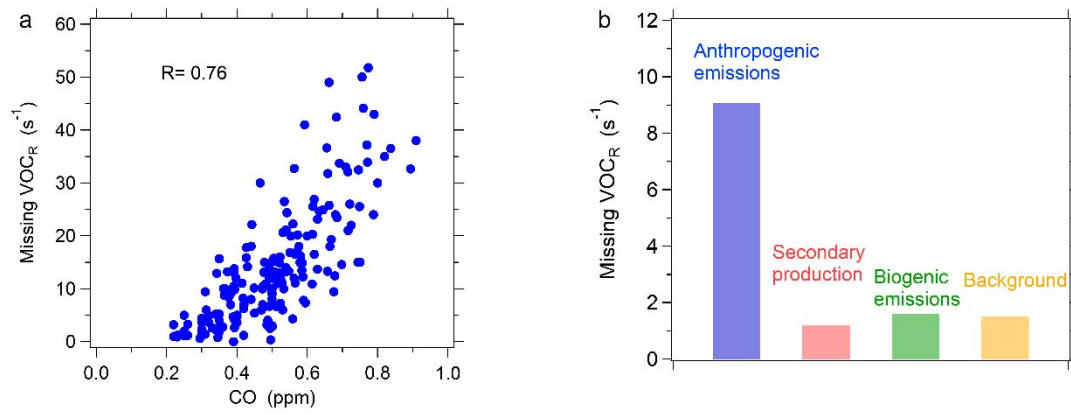
659 **and the error bars represent standard deviation.**

660



661

662



663

664 **Figure 3. The source apportionment of missing VOC<sub>R</sub> in high missing-VOC<sub>R</sub> days.**

665 (a) Correlation of missing VOC<sub>R</sub> with CO. Each point represents hourly data. (b)

666 Contributions of different sources to missing VOC<sub>R</sub> according to the MLR.

667

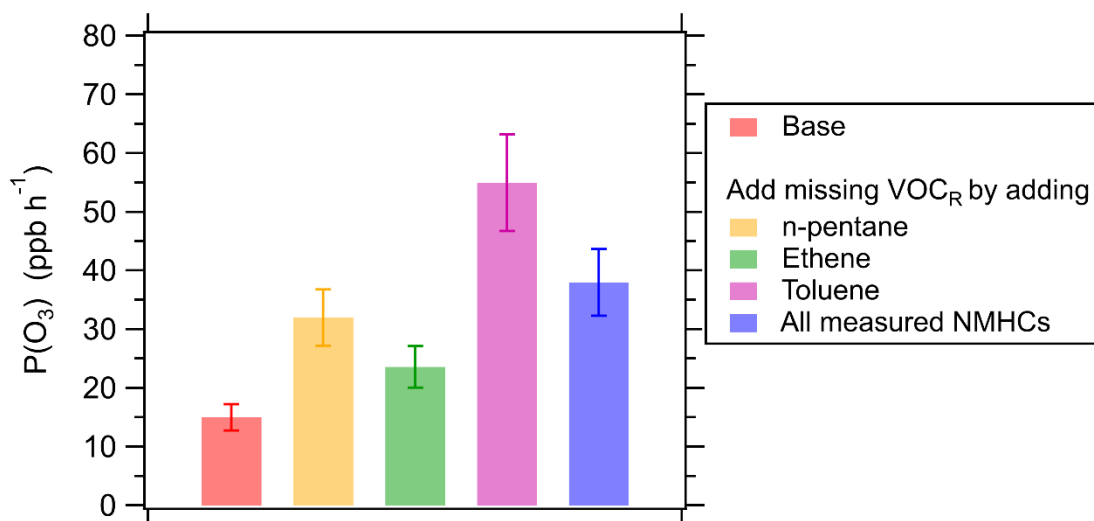


**Figure 4. Simulated daytime mean  $P(O_3)$  for the base scenario (without missing  $VO_{C_R}$ ) and the scenario considering missing  $VO_{C_R}$ , respectively, in high-missing  $VO_{C_R}$  days.** The missing  $VO_{C_R}$  is considered by adding individual species (n-pentane, ethene or toluene) or increasing all measured NMHCs to compensate for the missing  $VO_{C_R}$ . The error bar represents standard deviation of  $P(O_3)$  induced by the uncertainty of missing  $VO_{C_R}$ .

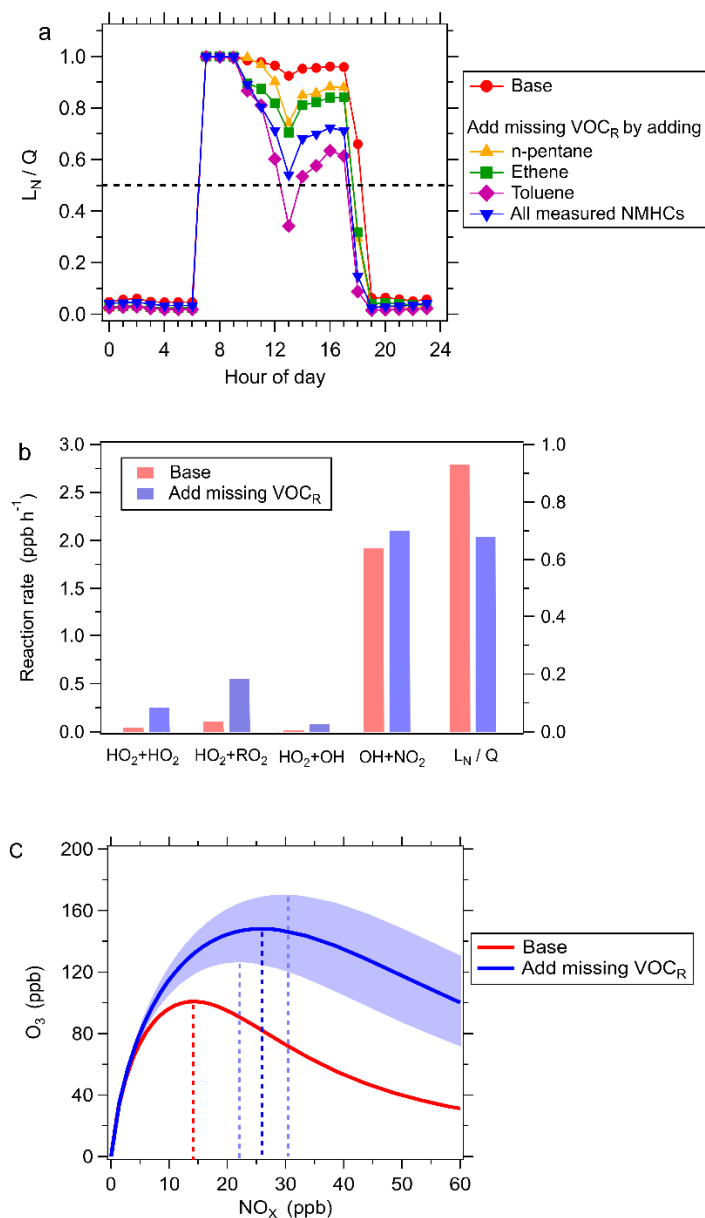


**Figure 5. The impact of missing VOC<sub>R</sub> on O<sub>3</sub> sensitivity for the high-missing VOC<sub>R</sub> days.** (a) Diurnal variations in  $L_N/Q$  for the base scenario and the scenarios considering missing VOC<sub>R</sub>. The missing VOC<sub>R</sub> is considered by adding individual species (n-pentane, ethene or toluene) or increasing all measured NMHCs to fill the missing VOC<sub>R</sub>. The dashed line represents the threshold value of  $L_N/Q$  that distinguishes VOC-limited and NO<sub>x</sub>-limited regimes. (b) The averages of radical sinks in the afternoon (12:00-18:00) for the base scenario (red bar) and the scenario considering missing VOC<sub>R</sub> (blue bar) by increasing all measured NMHCs to fill the missing VOC<sub>R</sub>. (c) Model-simulated dependence of daily peak O<sub>3</sub> concentrations on daily mean NO<sub>x</sub> concentrations for the

base scenario (red curve) and the scenario considering missing  $\text{VOC}_R$  (blue curve) by increasing all measured NMHCs to fill the missing  $\text{VOC}_R$ . The dashed lines parallel to Y-axis represent the threshold of  $\text{NO}_X$  levels to distinguish between VOC-limited and  $\text{NO}_X$ -limited regimes. The shaded area represents standard deviation induced by the uncertainty in missing  $\text{VOC}_R$ .